Graded structure of laser direct manufacturing bulk metallic glass

Lu, Yunzhuo; Huang, Yongjiang; Wu, Jing; Lu, Xing; Qin, Zuoxiang; Daisenberger, Dominik; Chiu, Yu Lung

DOI:
10.1016/j.intermet.2018.10.005

Graded structure of laser direct manufacturing bulk metallic glass

Yunzhuo Lu,[1,*] Yongjiang Huang,[2,*] Jing Wu,[3,*] Xing Lu,[1] Zuoxiang Qin,[1] Dominik Daisenberger,[4] Yu-Lung Chiu [3]

[1] *School of Materials Science and Engineering, Dalian Jiaotong University, Dalian 116028, China*
[2] *School of Materials Science and Engineering, Harbin Institute of Technology, Harbin 150001, China*
[3] *Department of Metallurgy and Materials, University of Birmingham, Edgbaston B15 2TT, UK*
[4] *Diamond Light Source, Harwell Science and Innovation Campus, Didcot, Oxfordshire, UK*

** Corresponding author: Tel.: +86-411-84105700; Fax: +86-411-84109417.*
**E-mail address: yunzhuohit@gmail.com (Yunzhuo Lu); yjhuang@hit.edu.cn (Yongjiang Huang); J.Wu.6@bham.ac.uk (Jing Wu)*

ABSTRACT

Extending the applications of metallic glasses for use as functionally graded materials could mitigate their intrinsic problems such as limited dimensions. Laser direct manufacturing (LDM) technology is an outstanding and reliable technique to fabricate structural-graded materials. Here, a $Zr_{50}Ti_5Cu_{27}Ni_{10}Al_8$ (Zr50) alloy was chosen as the model material to fabricate metallic glass by the LDM. By optimizing the LDM process through the finite-element simulation, a nearly fully amorphous Zr50 alloy with the thickness of larger than 10 mm was fabricated. The structural gradients, induced by gradual variation of crystallinity, were found in the deposited Zr50 metallic glass.

Keywords: laser direct manufacturing; bulk metallic glass; amorphous materials; functionally graded materials; laser deposition

1. Introduction

Metallic glasses have received considerable scientific and technological attentions due to their extraordinary mechanical and chemical properties[1-3]. However, the small dimensions of metallic glasses largely hinder their wide applications as structural materials [4, 5]. Extending the use of metallic glasses as functional materials could mitigate this problem [6, 7]. As a special class of functional materials, functionally graded materials, possess a number of advantages including an improved residual stress distribution, enhanced thermal properties, higher fracture toughness, and reduced stress intensity factors[8]. These advantages make them attractive in technological applications. Herein, a question arises: can we fabricate high performance structural-graded metallic glasses to overcome their "bottleneck" problems?

Consolidation of the amorphous powders into bulk materials, using the methods such as hot pressing[9], spark plasma sintering[10], injection[11], etc., is an effective way to fabricate metallic glass components. Among these methods, laser direct manufacturing (LDM) technology, which is a powder-based layer-by-layer shaping and consolidation process, allows us to finely tailor microstructure, porosity, shape and size of deposited materials[12-14]. The flexibility of structural design associated with the LDM makes it a reliable technique to fabricate structural-graded materials[15]. Moreover, comparing with the above mentioned powder metallurgy methods, LDM technology can produce metals having low levels of voids and porosity. At present, extensive works have been conducted on the LDM of metallic

glasses[16-19]. The cooling rates achieved by the LDM method can generally reach up to 10^3-10^4 K/s, significantly higher than the critical cooling rate required to produce an amorphous structure for most glass-forming alloy systems. This provides an opportunity to fabricate metallic glasses, even those with poor glass-forming ability, to overcome their size limitation. Moreover, the metallic glasses fabricated by the LDM method may essentially possess graded structures, which would be induced by the thermal history gradient along the building direction during the LDM process. In the previous works, however, most attention has been paid to the degree, characteristics and behaviors of the crystallization in the metallic glasses fabricated by LDM[20-22]. The graded structures, which would generate tremendous effects on the physical, chemical and mechanical properties of the LDM produced metallic glasses, have been ignored.

In the present work, a $Zr_{50}Ti_5Cu_{27}Ni_{10}Al_8$ (Zr50) alloy was chosen as the model material to fabricate large-size metallic glass by the LDM technology. The structural gradients, induced by the gradual variation of crystallinity, across the thin crystalline bands and along the building direction were found in the deposited Zr50 metallic glass. The microstructure and mechanical properties of the graded components were carefully studied. The formation mechanism of the graded structures was illustrated from the frame of thermal history. The gradient mechanical properties induced by the gradual crystallinity were also investigated in details.

2. Materials and methods

LDM of Zr50 metallic glass was performed using a coaxial powder feeding

LDM system. The laser source used in the experiments was IPG YLS 6000W SM CW ytterbium fiber laser with wavelength of 1070 nm. The schematic of the LDM process is shown in Fig. 1. The inset of Fig. 1 shows the outer appearance of a multi-layer 10-mm-thick Zr50 alloy sample fabricated by the LDM. The diameter, power and travel speed of the laser beam was 2 mm, 200 W and 800 mm/min, respectively. LDM experiments were conducted inside a working chamber, which is filled with argon gas to keep the oxygen level lower than 10 ppm. Argon atomized Zr50 powders in a size range of 20~50 μm were used for LDM process. Owing to the rapid solidification conditions, the majority of the particles produced by gas atomization in an argon atmosphere are spherical or near-spherical in shape. 45 carbon steel was selected as substrate materials due to its high yield strength and a relatively high thermal conductivity. Parallel tracks were partially overlapped with an overlap fraction of 30 %. The layer thickness in *z* direction during multi-layer deposition was set as 0.6 mm. The microstructure of deposited metallic glass samples was characterized using high energy synchrotron X-ray diffraction (HEXRD) and scanning electron microscope (SEM). The HEXRD experiments were carried out at beamline I15 of the Diamond Light Source, UK, using high energy, monochromatic X-rays with a photon energy of 76 keV. The X-ray beam was focused down to 70 μm in diameter and cleaned up with the pinhole directly in front of the sample. 2-dimensional XRD images were recorded using a Perkin-Elmer XRD1621 flat-panel detector positioned ～1 m from the sample. The scattering intensity $I(Q)$ versus scattering vector were extracted by integrating the obtained 2-D diffraction patterns along the radius of the diffraction circles in Q-space

using Data Analysis WorkbeNch (DAWN) software. The nanoindentation experiments were performed on the alloys at room temperature by an MTS Nanoindenter-XP, where the displacement and load resolution were lower than 0.1 nm and 50 nN. A professional finite-element simulation software, SYSWELD, is applied to calculate the thermal cycle curves in the present LDM processing. In the present study, the laser beam is modeled as a Gaussian distribution of heat flux from a moving heat source with a conical shape. The surface heat flux was assumed to be uniform during the process and produce a melt zone depth consistent with that experimentally observed. This heat flux corresponds to a laser power of 200 W and beam diameter of 2 mm. All the specific heat and thermal conductivity values used in the finite-element simulation are temperature-dependent, as described in our previous literature[23].

3. Results and discussion

The resulting microstructure of deposited samples is directly determined by the local thermal conditions, which are controlled by two key processing parameters in the LDM process, i.e., the laser power and the travel speed[24]. In order to obtain an ideal laser deposited Zr50 sample with fully or nearly fully amorphous microstructure, the processing parameters are optimized by using the finite-element method (FEM) analysis and the time-temperature-transformation (TTT) diagrams of the Zr50 alloy. The TTT-diagram estimation and FEM simulation in details were prescribed in our recent published paper [23]. To optimize the LDM processing parameters, single-track Zr50 alloy were printed on a Zr50 metallic glass substrate. The cross-sectional

microstructure of the single-track deposited Zr50 alloy sample is shown in the left part of Fig. 2. The laser travel direction is perpendicular to the plane of the images. Three different regions can be easily distinguished, namely the molten pool in the upper part, the crystalline heat-affected zone (HAZ (crystalline)) in the middle part, and the metallic glass substrate in the lower part. For comparison, we analyze the crystallization of all the nodes of finite element mesh in the cross section of the FEM-simulated single-track Zr50 alloy. The crystalline positions are indicated by red dots. The spatial distribution of crystallization obtained from the FEM analysis is shown in the right part of Fig. 2. Clearly, the distributions of crystallization calculated by our method agree well with the experimental observations, confirming the validity of our method to predict the crystallization in the LDM of Zr50 metallic glass. Then, the ratios of the crystalline area to the total area shown in right part of Fig. 2 are calculated to evaluate the crystallinity of the deposited Zr50 metallic glass. A combination of laser power of 200 W and travel speed of 800 mm/min is found to present the lowest crystalline fraction. Thus, the laser power of 200 W and travel speed of 800 mm/min are chosen as the optimum LDM parameters to fabricate large-sized Zr50 alloy samples.

A typical microstructure of a deposited 10-mm-thick Zr50 alloy perpendicular to the laser travel direction is shown in Fig. 3(a). Featureless light gray regions, corresponding to amorphous zones, are observed surrounded by thin dark gray crystalline bands. From Fig. 3(a) we can note that the thin gray bands take lower than 5% of the total cross area, indicating the deposited Zr50 alloy with the thickness of

larger than 10 mm contains lower than 5 vol.% crystalline phases. More inspiringly, the widths of dark gray crystalline bands remain almost unchanged with increasing the deposited layers, indicating that the deposited Zr-based alloy does not crystallize more seriously as the sample becomes thicker. Therefore, using the present processing parameters can produce Zr50 metallic glass without dimensional limitation.

To study the structural evolution of the laser deposited Zr50 alloy sample along the building direction, nanoindentation was performed from bottom to the top along the red dot line shown in Fig. 3(a). The spacing between two neighboring indents is set as 20 μm. The hardness was calculated by Oliver-Pharr method[25]. The hardness measured at different heights along the red dot line is plotted in Fig. 3(b). As presented, the hardness firstly increases and then decreases with increasing the height in local regions, while the hardness exhibits an overall decreasing trend. This hardness trend may be correlated with the crystallinity of the deposited Zr50 alloy sample, since the crystallization caused by annealing would enhance the hardness of metallic glass[26, 27]. For instance, four typical crystalline regions I, II, III and IV shown in Fig. 3(a) possess higher hardness than their neighbouring amorphous regions, as denoted by blue bands in Fig. 3(b).

To further study the graded structures of the laser deposited Zr50 alloy sample, HEXRD experiments were performed across a typical thin crystalline band. Four positions ①-④ illustrated in Fig. 4(a) were chosen to perform the HEXRD tests. A typical diffraction pattern taken at position 1 is shown in Fig. 4(b). Figure 4(c) displays the corresponding $I(Q)$ curves measured at the four positions. The absence of

any sharp diffraction peaks at the positions 1 and 4 proves their fully amorphous structure. Their intensity curves consist of a broad diffraction peak at 2.71 $Å^{-1}$ followed by a smaller one at 4.48 $Å^{-1}$. The inset highlights the top part of the first peaks for curves 1 and 4. Clearly, $I(Q)$ curve of position 1 possesses a higher Q value than that of position 4, indicating the shortening of the distance between constituent atoms for the lower part of the deposited Zr50 alloy sample[28]. During the LDM process, the lower parts of the deposited sample experience more thermal cycles than the upper ones. Then the glass structure of the lower part relaxes more severely towards equilibrium. More excess free volume thus annihilate, resulting in the densification of the glassy phase and the shortening of the atomic distance. It can also be noticed from Fig. 4(c) that sharp Bragg peaks, corresponding to crystalline phases, appear in the $I(Q)$ curves at the positions 2 and 3. The Bragg peak positions remain almost unchanged for these two positions, whereas the intensities increase from position 2 to position 3. The above results suggest that the crystalline content increases firstly and then decreases cross the thin crystalline band.

To elucidate the gradual crystallinity across crystalline thin bands, the typical thermal cycle curves during the LDM process at the nodes of finite element mesh along the green line shown in Fig.2 are presented in Fig.5(a). The TTT diagrams upon heating and cooling of the Zr50 metallic glass are also proposed in this figure. The inset of Fig.5(a) magnifies the region indicated by the dotted box shown in Fig.5(a). We just show the thermal cycle curves corresponding to the positions in the thin crystalline band in the inset of Fig.5(a). Obviously, the overlapping between the

thermal cycle curve and the crystallization curve of TTT diagram upon heating gradually decreases with the distance away from the melting zone. A larger overlapping between the thermal cycle curve and the crystallization curve of TTT diagram indicates that there is more time for the formation of new crystal nuclei and time for crystals to grow[29]. Thus, the crystallinity in thin crystalline band gradually decreases with the distance away from the melting zone. In addition, the already formed crystals in the thin crystalline band would act as the heterogeneous nucleation sites for crystallization formation at the bottom of the melt zone that is very close to the crystalline thin band[30]. Then some crystalline phases can also be found at the bottom of the melt zone. With distance away from the thin crystalline band, the crystallinity in the bottom of the melt zone also gradually decreases. Therefore, the crystallinity in the regions across crystalline thin bands increases firstly and then decreases from the bottom up.

For the thin crystalline bands located at different heights of the deposited Zr50 metallic glass, the gradual variations of the crystallinity along the building direction may be correlated with the gradient accumulated structural relaxation. To account for this, we draw a schematic of the cross section for the LDM of Zr50 metallic glass, as presented in Fig. 5(b). The red thin bands and yellow regions refer to the crystalline and amorphous phase, respectively. We calculate the thermal cycle curves of the point A (shown in the schematic of Fig. 5(b)) during the LDM process of a 5-layer Zr50 metallic glass by FEM simulation. Each layer consists of 5 tracks. The relative positions of the multiple tracks are shown in the schematic of Fig. 5(b). The thermal

cycle curve of the point A is presented in Fig. 5(d). The numbers shown in Figs. 5 (b) and (d) denote the track sequence. For the first track, the deposited metallic glass is vitrified from the molten liquid. No crystallization takes place at point A in this process, since the cooling curve of track 1 does not intersect with the crystallization curve of TTT diagram upon cooling, as shown in Fig. 5(c), which presents the thermal cycle curves of point A after some typical tracks and the TTT diagram of Zr50 metallic glass. After the first track, the subsequent tracks will accumulate the structural relaxation for the Zr50 metallic glass formed at the first track through the heat transfer. The accumulated structural relaxation can cause the formation of the region with more serious crystalline degree[31]. In addition, the enough accumulated structural relaxation can also facilitate the crystallization of the amorphous region. Many previous isothermal annealing experiments have shown that the annealing temperature below or above the glass transition temperature (T_g) can cause a tremendous difference in the structural relaxation and its induced crystallization. For instance, several hours is required for the crystallization of the $Zr_{41.2}Ti_{13.8}Cu_{12.5}Ni_{10}Be_{22.5}$ metallic glass when annealed below or at T_g[32]. Contrarily, only few seconds is required for metallic glass when annealed at temperatures higher than T_g [18]. The annealing temperatures above T_g are more effective in relaxing the nonequilibrium amorphous structure. Then the thermal cycle whose maximum temperature is higher than T_g is named as effective thermal cycle (ETC) in the present work. The ETCs of point A during the LDM process are marked by red arrows in Fig. 5(d). There are five ETCs for point A. However, the crystallization of point A is just

induced by the track 6. This is because in these ETCs, only the thermal cycle curve of track 6 overlaps with the crystallization curve of TTT diagram upon heating, as shown in Fig. 5(c). The subsequent ETCs of point A caused by tracks 7 and 11 cause more serious crystalline after track 6. For point C shown in the schematic of Fig. 5(b), its amorphous structure forms at track 16 and crystallizes after track 21. It experiences only one ETC after crystallization which induced by the depositing of track 22. Then the crystallinity of point C is lower than that of point A. For point B, its thermal cycle curves during the LDM process are identical to the first four thermal cycle curves of point A, as presented in Fig. 5(d). Both the point A and point B experience two ETCs after the crystallization. However, their crystallinity is still slightly different, since point A experiences five more thermal cycles produced by the five tracks of the fifth layer, i.e., the five thermal cycle curves of the five layers shown in Fig. 5(d). Though these five thermal cycle curves with the annealing temperatures lower than T_g, they also contribute to the accumulation of structural relaxation. Therefore, in the deposited Zr50 metallic glass, the crystallization gradually decreases from the bottom to the upper part.

4. Conclusions

In summary, a Zr50 metallic glass was chosen as the powder materials to fabricate large-sized metallic glass by using the LDM technology. A 10-mm-thick Zr50 metallic glass containing lower than 5 vol% crystalline phases was then successfully fabricated. The structural gradients, induced by the gradual variation of crystallinity, across the thin crystalline bands and along the building direction were

found in the deposited Zr50 metallic glass. The gradual variation of crystallinity was mainly due to the gradient structural relaxation accumulation induced by the thermal history.

Acknowledgements

The authors would like to acknowledge the financial supports from the National Natural Science Foundation of China under Grant Nos. 51671042, 51401041, 51671043 and 51671070.

References

[1] M. Chen, NPG Asia Mater. 3 (2011) 82-90.
[2] A. Greer, E. Ma, MRS Bull. 32 (2007) 611-619.
[3] H. Y. Fan, X. J. Liu, H. Wang, Y. Wu, H. Wang, Z. P. Lu, Intermetallics 90 (2017) 159-163.
[4] W. L. Johnson, MRS Bulletin 24 (1999) 42-56.
[5] C. T. Liu, Z. P. Lu, Intermetallics 13 (2005) 415-418.
[6] W.H. Wang, Adv. Mater. 21 (2009) 4524-4544.
[7] B. Huang, Y. Yang, A. D. Wang, Q. Wang, C. T. Liu, Intermetallics 84 (2017) 74-81.
[8] Y. Miyamoto, W. Kaysser, B. Rabin, A. Kawasaki, R.G. Ford. Functionally graded materials: design, processing and applications, MA: Kluwer Academic Publishers; 1999.
[9] P. Lee, M. Kao, C. Lin, J. Huang, Intermetallics 14 (2006) 994-999.
[10] G. Xie, F. Qin, S. Zhu, A. Inoue, Intermetallics 29 (2012) 99-103.
[11] A. Wiest, J.S. Harmon, M.D. Demetriou, R.D. Conner, W.L. Johnson, Scr. Mater. 60 (2009) 160-163.
[12] D. Herzog, V. Seyda, E. Wycisk, C. Emmelmann, Acta Mater. 117 (2016) 371-392.
[13] J.J. Lewandowski, M. Seifi, Annu. Rev. Mater. Res. 46 (2016) 151-186.
[14] W. Chen, L. Thornley, H.G. Coe, S.J. Tonneslan, J.J. Vericella, C. Zhu, E.B. Duoss, R.M. Hunt, M.J. Wight, D. Apelian, Appl. Phys. Lett. 110 (2017) 094104.
[15] X. Tan, Y. Kok, Y.J. Tan, M. Descoins, D. Mangelinck, S. B.Tor, K. F. Leong, C. K. Chua, Acta Mater. 97 (2015) 1-16.
[16] X.P. Li, Adv. Eng. Mater. (2017) 1700874.
[17] D. Ouyang, N. Li, W. Xing, J. Zhang, L. Liu, Intermetallics 90 (2017) 128-134.
[18] C. Yang, C. Zhang, W. Xing, L. Liu, Intermetallics 94 (2018) 22-28.
[19] S. Pauly, L. Löber, R. Petters, M. Stoica, S. Scudino, U. Kühn, J. Eckert, Mater. Today 16 (2013) 37-41.
[20] Y. Shen, Y. Li, H. L. Tsai, J. Non-Cryst. Solids 481 (2018) 299-305.
[21] H. Sun, K. Flores, J. Mater. Res. 23 (2008) 2692-2703.

[22] H. Sun, K.M. Flores, Intermetallics 43 (2013) 53-59.
[23] Y.Z. Lu, H. Zhang, H.G. Li, H.D. Xu, G.K. Huang, Z.X. Qin, X. Lu, J. Non-Cryst. Solids 461 (2017) 12-17.
[24] D. Gu, W. Meiners, K. Wissenbach, R. Poprawe, Int. Mater. Rev. 57(3) (2012) 133-164.
[25] W.C. Oliver, G.M. Pharr, J. Mater. Res. 19 (2004) 3-20.
[26] J. Basu, N. Nagendra, Y. Li, U. Ramamurty, Philos. Mag. 83 (2003) 1747-1760.
[27] Z. Zhang, J. Xie, Mater. Sci. Eng. A 407 (2005) 161-166.
[28] Y. Huang, J. Khong, T. Connolley, J. Mi, Appl. Phys. Lett. 104 (2014) 031912.
[29] J. Schroers, Adv. Mater. 22 (2010) 1566-1597.
[30] A. Gebert, J. Eckert, L. Schultz, Acta Mater. 46 (1998) 5475-5482.
[31] E. Goncharova, R. Konchakov, A. Makarov, N. Kobelev, V. Khonik, J. Non-Cryst. Solids 471 (2017) 396-399.
[32] C. Suryanarayana, A. Inoue. Bulk metallic glasses, CRC press, 2010.

Figure captions

Figure 1 Schematic of the LDM process. The inset shows the outer appearance of a multi-layer 10-mm-thick Zr50 alloy sample fabricated by the LDM.

Figure 2 The left part is a SEM image showing the microstructure in the cross section of the single-track deposited Zr50 alloy sample, the right part is the spatial distribution of crystallization obtained from the FEM analysis.

Figure 3 (a) SEM image describing a typical microstructure of the deposited 10-mm-thick Zr50 alloy perpendicular to the laser travel direction. (b) The hardness measured at different heights along the red dot line shown in (a).

Figure 4 (a) The schematic of four relative positions ①-④ that conduct HEXRD experiments. (b) A typical diffraction pattern taken at position ①. (c) The corresponding *I*(Q) curves measured at the four positions.

Figure 5 (a) Thermal cycle curve during the LDM process at the nodes of finite element mesh along the green line shown in Fig.1(c). (b) A schematic of the cross section for the LDM of a five-layer Zr50 metallic glass. (c) The thermal cycle curves of point A after some typical tracks and the TTT diagram of Zr50 metallic glass. (d) The thermal cycle curve of the point A. The numbers shown in (b) and (d) denote the track sequence.

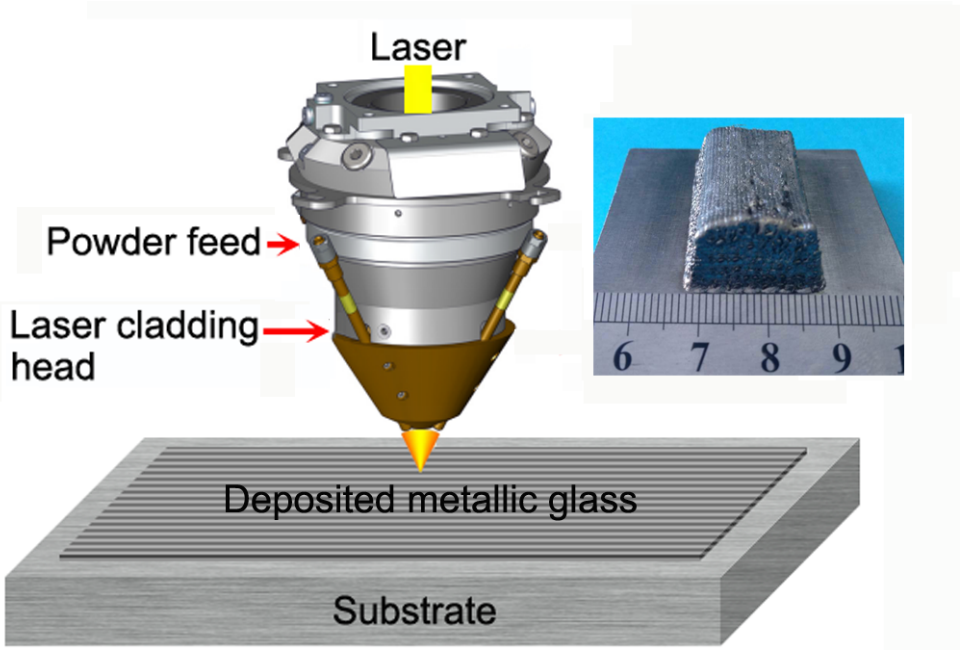
Laser
Powder feed
Laser cladding head
6 7 8 9
Deposited metallic glass
Substrate

Figure 1

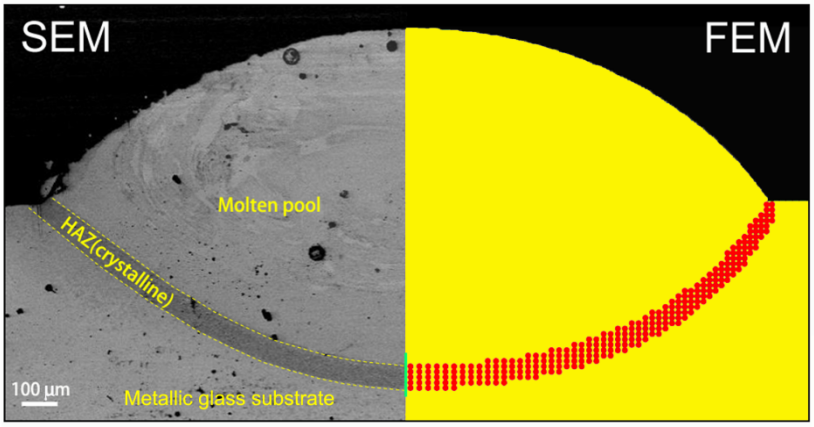
SEM
FEM
Molten pool
HAZ(crystalline)
100 μm
Metallic glass substrate

Figure 2

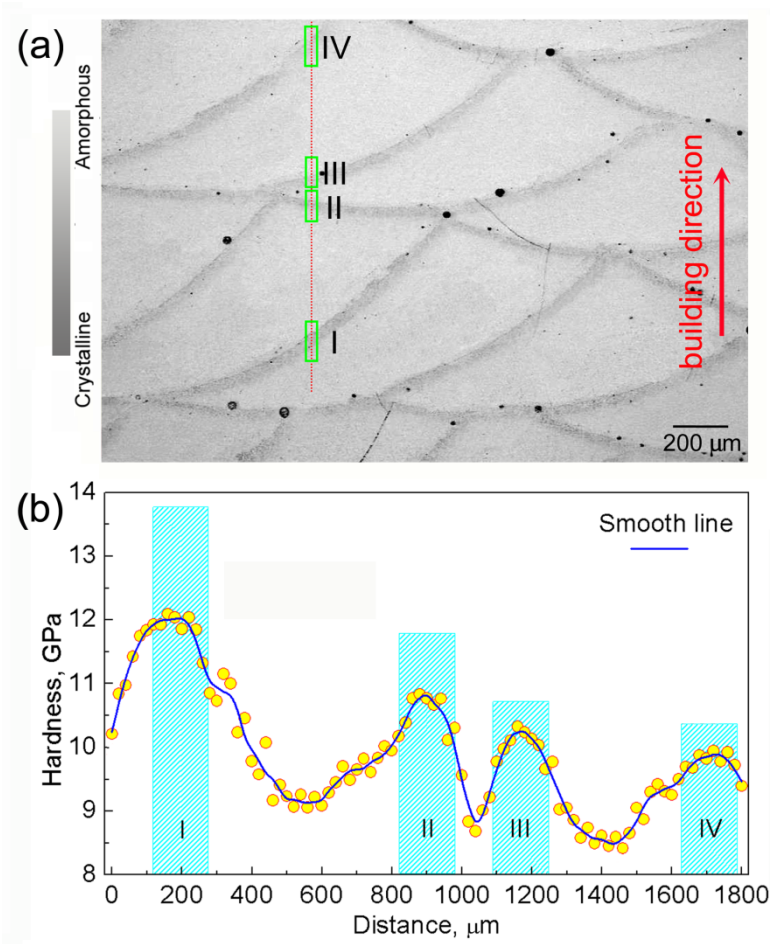
(a)
Amorphous
Crystalline
IV
III
II
I
building direction
200 μm
(b)
Smooth line
Hardness, GPa
14
13
12
11
10
9
8
I
II
III
IV
0
200
400
600
800
1000
1200
1400
1600
1800
Distance, μm

Figure 3

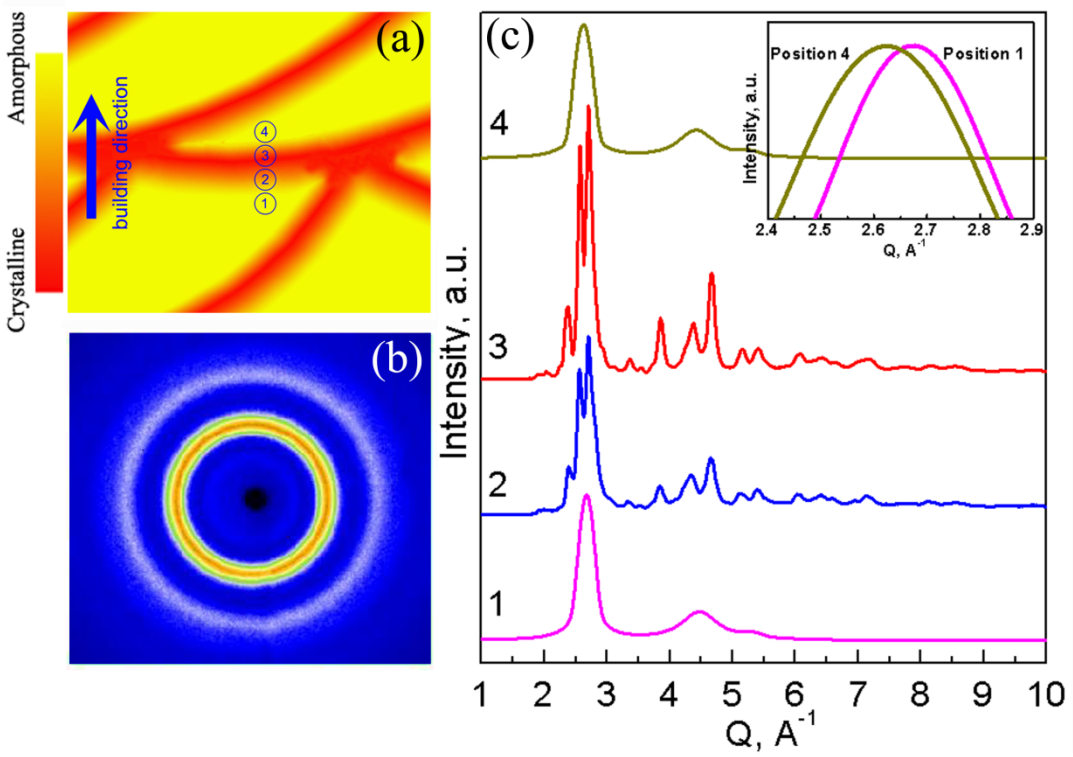
Amorphous
Crystalline
(a)
building direction
4
3
2
1
(b)
(c)
4
3
2
1
Intensity, a.u.
Position 4
Position 1
Intensity, a.u.
2.4
2.5
2.6
2.7
2.8
2.9
Q, A-1
1
2
3
4
5
6
7
8
9
10
Q, A-1

Figure 4

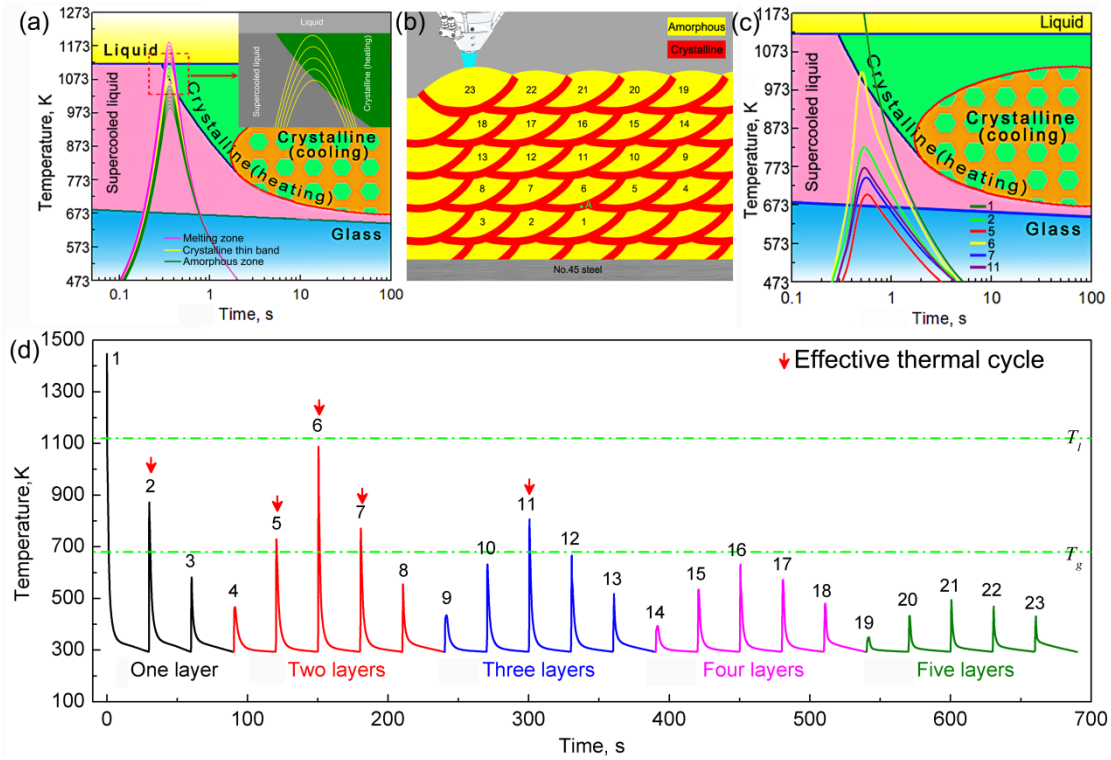
(a)
Liquid
Supercooled liquid
Crystalline (heating)
Crystalline (cooling)
Glass
Melting zone
Crystalline thin band
Amorphous zone
Temperature, K
Time, s
(b)
Amorphous
Crystalline
No.45 steel
(c)
Liquid
Supercooled liquid
Crystalline (heating)
Crystalline (cooling)
Glass
Temperature, K
Time, s
(d)
Effective thermal cycle
T_l
T_g
One layer
Two layers
Three layers
Four layers
Five layers
Temperature,K
Time, s

Figure 5